ADVANCED ELECTRONIC MATERIALS
www.advelectronicmat.de

Flexible Asymmetric Microsupercapacitors from Freestanding Hollow Nickel Microfiber Electrodes

*Ahiud Morag and Raz Jelinek**

The increasing demand for flexible and wearable microelectronics is a major driving force for the development of high-performance small-volume energy sources. Microsupercapacitors exhibit significant potential in energy storage as they provide high power and good cycle stability. Yet, most microsupercapacitors display low energy densities limiting their practical use in microelectronics. Here, synthesis of high surface area freestanding electrodes comprising hollow nickel microfibers is demonstrated. The microfiber nickel electrodes constitute a platform for flexible asymmetric microsupercapacitors exhibiting excellent mechanical resilience as well as high energy density (0.11 mWh cm^{-2}) and power density (37.5 mW cm^{-2}). The freestanding nature and extensive surface area of the electrodes contribute to pronounced areal and volumetric capacitance, energy storage values, and stability after numerous (hundreds) physical bending cycles. The simple preparation scheme and use of an inexpensive building block (e.g., nickel) underscore potential uses as light and flexible energy storage devices.

1. Introduction

Flexible microelectronics is a rapidly expanding field encompassing diverse applications, including sensors, health-monitoring patches, and energy-harvesting devices.[1–5] Flexible microelectronic devices usually require the use of microbatteries as energy sources. Current battery designs are mostly based upon lithium-ion (Li-ion) technologies.[6,7] Li-ion microbatteries, however, suffer from a low power density and low cycle stability[8,9] and alternative technologies are intensively pursued. In this context, *micorsupercapacitors (MSCs)* have emerged as promising substituents for energy storage.[10,11] MSCs, based on either electric double-layer capacitance[12,13] or fast faradaic redox reactions (i.e., pseudo-capacitance),[14] exhibit higher power densities compared with Li-ion batteries, and can withstand numerous charge/discharge cycles.[15] However, MSCs display very low energy densities due to the fact that only the surfaces of the electrochemically active material participate in the electrochemical reactions;[10,14] this limitation has prevented wide applicability of MSCs for energy storage in microelectronics.

Planar MSCs composed of interdigitized electrodes have been proposed as viable technological solutions for energy storage devices. Such electrodes facilitate rapid diffusion of molecules participating in the redox reactions; they are also generally thin and accordingly can be integrated in microelectronic devices.[16–18] However, such MSCs also exhibit practical limitations since in many instances they do not contain sufficient electrochemical surface areas. Several studies have addressed these issues by fabricating planar MSCs using porous carbon ink,[17] laboratory filter paper,[19] and electrostatic spraying of reduced graphene oxide (rGO) and carbon nanotube mixtures.[20] Yet, such processes are elaborate and often produce devices exhibiting low energy densities.

Other strategies have focused on chemical means for creation of porous electrode exhibiting high surface areas, serving as a scaffold for deposition of the electrochemically active material.[21,22] Varied porous-electrodes have been reported, comprising, for example, Au nanostructures,[23] carbon cloth,[24] aligned carbon nanotubes,[25] and nickel foam.[26] While such electrode designs provide high capacitance, they usually exhibit considerable thickness,[23–26] making them less suitable for integration in microelectronics. Recent studies have shown that deposition of *nickel* on various substrates yield high surface area electrodes, which are particularly attractive because of the very low cost of Ni compared with other metals employed in electrode fabrication.[27–29] Yet, even in those systems, removal of the electrode substrate-supports was difficult, thereby limiting their usefulness.

In addition to energy consideration, *flexibility* is another crucial aspect in varied microelectronic devices. Thin MSCs that can withstand folding without significant degradation in performance are highly sought.[30,31] While MSCs exhibiting high flexibility and mechanical resilience have been reported, they are either too bulky,[27,32] or the devices display limited electrochemical performance.[19,33] Indeed, construction of flexible, thin electrodes which can also provide high energy and power densities in MSCs is still a significant challenge.

In this work, we demonstrate construction of an innovative MSC device consisting of hollow nickel microfiber electrodes. The electrodes were prepared by electroless deposition of nickel on carboxylated polystyrene (PS), followed by Ni electrodeposition. Further coating of either MnO_2 or a mixture of polypyrrole

A. Morag, Prof. R. Jelinek
Department of Chemistry and Ilse Katz Institute for Nanoscale Science and Technology
Ben-Gurion University
Beer-Sheva 8410501, Israel
E-mail: razj@bgu.ac.il

The ORCID identification number(s) for the author(s) of this article can be found under https://doi.org/10.1002/aelm.201800584.

DOI: 10.1002/aelm.201800584

 © 2018 WILEY-VCH Verlag GmbH & Co. KGaA, Weinheim

(PPy) and rGO generated high areal capacitance electrodes. An asymmetric MSC (AMSC) device was assembled, using MnO_2-coated electrode as the cathode and PPy/rGO as the anode, exhibiting high areal energy density and power density, further displaying excellent mechanical stability and flexibility.

2. Results and Discussion

2.1. Nickel Microfiber Electrode Synthesis and Characterization

Figure 1 illustrates the fabrication process of the porous hollow Ni microfiber electrode. The procedure starts with generation of PS microfibers through electrospinning, employing a PS/dimethylformamide (DMF) solution (Figure 1A).[34] The PS microfibers were subsequently annealed at 100 °C to provide more pronounced interfaces between microfibers and enhance film stability. This was followed by carboxylation of the PS microfibers' surfaces using $KMnO_4$;[35] the carboxylic residues constitute nucleation sites for the subsequent electroless deposition nickel, generating a thin-layer Ni coating.[36] As indicated in Figure 1, the electroless Ni-coated PS microfibers were further subjected to Ni electrodeposition designed to increase the stability and conductivity of the nickel layer. A final step of toluene-induced dissolution of the PS cores yielded a freestanding electrode comprising an interspersed network of hollow metallic nickel microfibers.

Figure 2 depicts microscopic and electrical characterization of the nickel electrode, underscoring the unique hollow microfiber morphology, flexibility, and mechanical resilience. Scanning electron microscopy (SEM) images in Figure 2A–C show the intertwined network of highly uniform Ni microfibers, exhibiting outer diameters of 3.4 ± 0.6 μm and inner diameter of 1.8 ± 0.2 μm. Importantly, Figure 2A demonstrates that ample space exists between the Ni microfibers—crucial for allowing efficient diffusion of electrolyte ions within the MSC.[37,38] The SEM image in Figure 2B further confirms that the microfibers adopt a continuous Ni coating. The cross-sectional image in Figure 2C reveals an overall electrode thickness of approximately 25 μm and highlights the remarkable hollow morphology of the Ni microfibers. Attesting to the high surface area of the Ni microfiber electrode, the areal density of 6 mg cm^{-2} is lower than scaffolds used in recently reported electroless-deposited nickel electrodes.[19,27]

The mechanical resilience of the hollow microfiber Ni electrode upon physical deformation was evaluated (Figure 2D,E). Figure 2D depicts the effects of *bending* and *twisting* upon the electrical resistance of an ≈2.0 × 0.5 cm^2 electrode. Importantly, as shown in Figure 2D, the electrode exhibited less than 1% resistance change even upon significant physical deformations. Similarly, very small resistance changes were apparent upon application of 800 bending cycles (Figure 2E). Overall, the data in Figure 2D,E attest to the extraordinary mechanical and electrical stability of the hollow Ni microfiber network.

2.2. Fabrication of Electrodes for an Asymmetric Microsupercapacitor (AMSC)

The hollow Ni microfiber electrode was used as a freestanding conductive substrate for construction of both cathode (**Figure 3**) and anode (**Figure 4**) in a flexible AMSC. Figures 3 and 4 present morphological and electrochemical characterization of the two electrodes—MnO_2-coating Ni microfibers in case of the cathode (Figure 3) and PPy/rGO for the anode (Figure 4). Electrodeposition of MnO_2 was carried out using manganese acetate as the precursor;[27] X-ray photoelectron spectroscopy (XPS) analysis confirmed that the deposited layer indeed comprised of MnO_2 (Figure S1, Supporting Information).[39] The SEM images in Figure 3A indicate that the microfiber morphology was preserved after coating with MnO_2. While the SEM analysis in 3A shows that the overall porosity of the electrode was reduced compared with the bare Ni microfiber network (e.g., Figure 2A) due to the MnO_2 deposition, the appearance of cracks in the MnO_2 layer (also reported, for example, in RuO_2-coated Au electrodes[23]) contributes to high electrochemical surface area and diffusion of the electrolyte within the MnO_2 layer. The high-magnification SEM image of the MnO_2 layer in Figure 3A,iii reveals nanoscale surface roughness, further increasing the electroactive surface area of the electrode.[21] Cross-sectional SEM image of the MnO_2-coated Ni electrode shows uniform coating over the entire Ni electrode with just a small increase in the overall thickness of the electrode (Figure S2, Supporting Information).

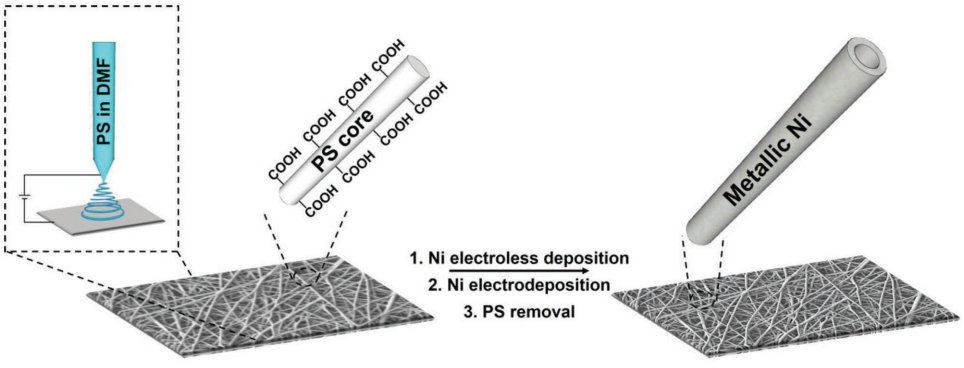

Figure 1. Fabrication of the hollow nickel microfiber electrode. Polystyrene (PS) fibers are deposited via electrospinning (left inset); the PS fibers are carboxylated, and coated with nickel via combined electroless deposition and electrodeposition. Final dissolution of the PS cores through application of toluene yields a network of hollow metallic nickel microfibers.

© 2018 WILEY-VCH Verlag GmbH & Co. KGaA, Weinheim

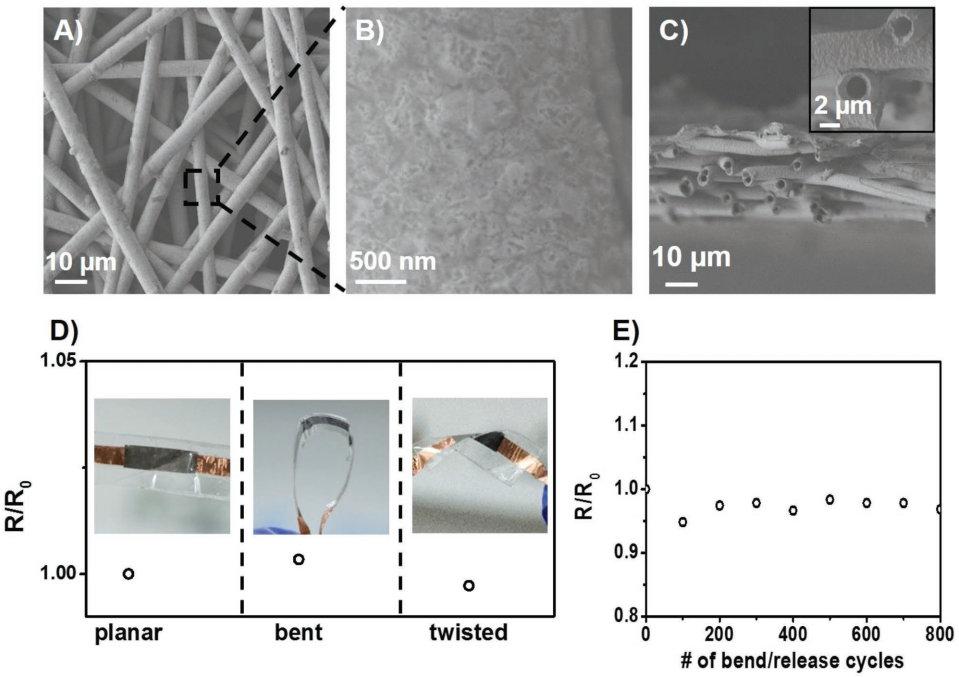

Figure 2. Characterization of the hollow Ni microfiber electrode. A,B) Top view scanning electron microscopy (SEM) images of the Ni electrode. C) Cross-sectional SEM image of the Ni electrode. The inset shows high magnification of individual hollow wire. D) Relative resistance of the Ni electrode upon bending and twisting; the photographs depict the configuration analyzed. R_0 corresponds to the initial measured resistance of the planar electrode. E) Relative resistance of the Ni electrode as a function of bending cycles.

Figure 3B,C depicts the electrochemical properties of the MnO_2-coated Ni microfiber electrode. The experiments were carried out in a three-electrode system using 1 M Na_2SO_4 solution as the electrolyte. Figure 3B,i presents the cyclic voltammetry (CV) curves recorded at different scan rates. At low scan rate, the shape of the curve is almost rectangular (Figure S3, Supporting Information), indicating pseudocapacitive behavior. The graph in Figure 3B,ii demonstrates that a high areal capacitance of 1200 mF cm^{-2} was obtained at a low scan rate of 1 mV s^{-1}; when the scan rate was increased to 100 mV s^{-1}, the capacitance decreased to 170 mF cm^{-2}. Capacitance decrease and concomitant loss of rectangular shapes of the CV curves are common upon high loading of the active materials in pseudocapacitors and ascribed to the higher resistance developed in the pseudocapacitive layer.[27,40] Nevertheless, the capacitance exhibited by the MnO_2-coated Ni microfiber electrode exhibits superior performance compared with recently reported thin-film supercapacitor electrodes.[33,41,42]

The galvanostatic charge/discharge curves in Figure 3C indicate high areal capacitance of 1150 mF cm^{-2} at a current density of 5 mA cm^{-2} (Figure 3C,ii). Increasing the current density to 25 mA cm^{-2} yielded more than 50% capacitance retention, underscoring potential use of the electrode in high-power microelectronics applications. Indeed, the pronounced capacitance retention at high current density, which translates to high charge/discharge rate, is on par or greater than previously reported thin electrodes.[33,43] Based upon impedance measurements in a frequency range of 100 kHz–10 mHz, the calculated electrolyte resistance and charge transfer resistance of the electrode were 0.4 and 1.17 Ω cm^2, respectively (Figure S4, Supporting Information); the almost linear dependence at low frequencies indicates a near-ideal capacitor behavior.[27,40] Cycle stability measurements of the electrode yielded 110% retention after 5000 cycles (Figure S5, Supporting Information). This capacitance increase is attributed to electrode wetting and results in more effective participation of the active material in the electrochemical reactions.[44,45]

In order to assemble a complete AMSC, preparation of the anode through electrodeposition of a mixture of PPy and rGO was carried out (Figure 4).[46] Similar to the MnO_2-coated Ni cathode (Figure 3A), surface analysis of the PPy/rGO-coated Ni electrode confirms that the microfiber network was retained (Figure 4A). Specifically, the electrode surface displayed intertwined rGO sheets coated with PPy, yielding a high electrochemical surface area. In addition, much the same as the MnO_2-coated cathode (e.g., Figure 3A), PPy/rGO treatment did not disrupt the hollow microfiber morphology of the Ni electrode (Figure S6, Supporting Information). XPS analysis verified the PPy coating in the electrode (Figure S7, Supporting Information).[47]

Electrochemical analysis of the PPy/rGO-coated Ni electrode shows capacitance values comparable to the MnO_2-coated cathode at low charge/discharge rates (Figure 4B,C; Figure S8, Supporting Information). While the MnO_2-coated electrode did not give rise to distinct oxidation–reduction peaks (Figure S3, Supporting Information), the PPy/rGO-coated electrode featured such peaks at −0.3 and −0.5 V (Figure S8, Supporting Information), ascribed to the PPy layer.[46] It should be noted that when higher charge/discharge rates were examined, the capacitance of the PPy/rGO-coated Ni anode decreased faster than the MnO_2-coated cathode (Figure 4B,ii), attributed to

© 2018 WILEY-VCH Verlag GmbH & Co. KGaA, Weinheim

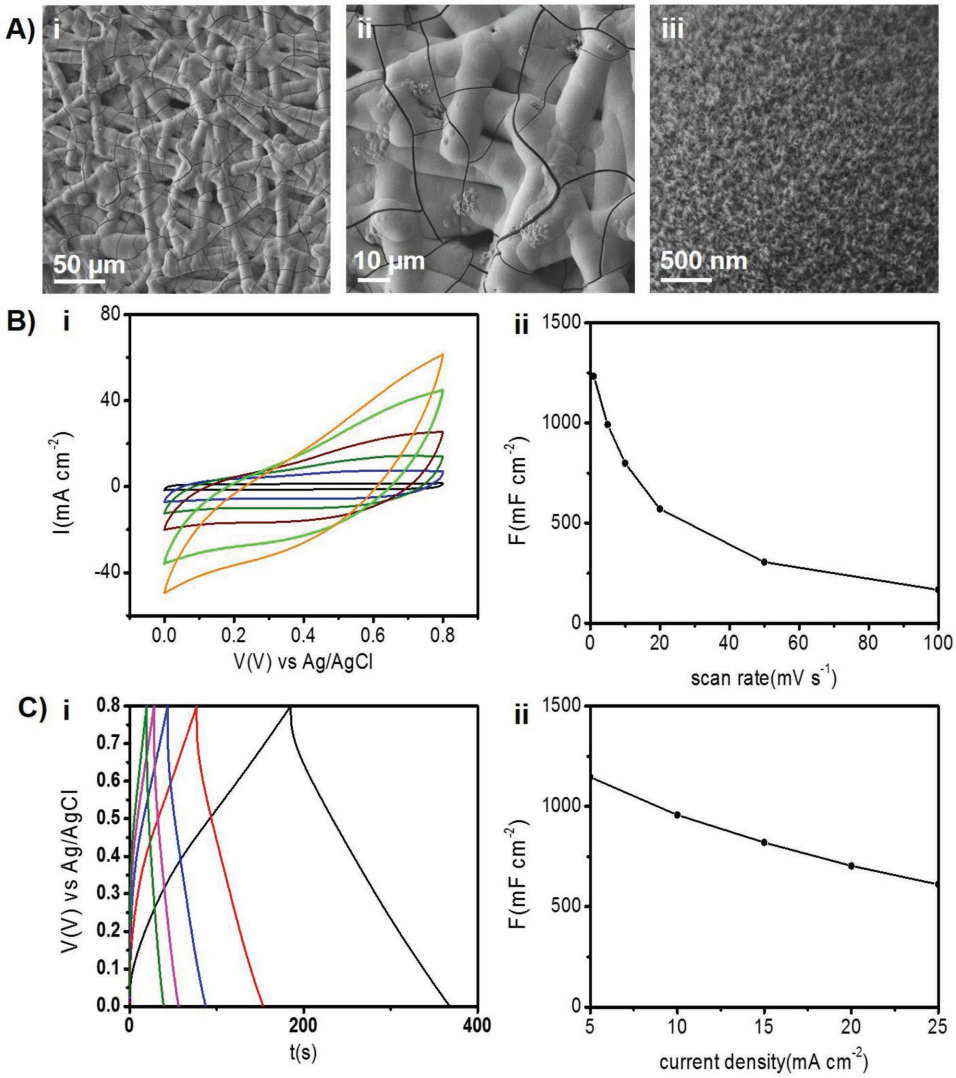

Figure 3. Characterization of the MnO_2-coated Ni electrode. A) SEM images of the MnO_2-coated Ni microfiber network at different scales. B.i) Cyclic voltammetry curves of the electrode using 1 M Na_2SO_4 as the electrolyte at scan rates of 1, 5, 10, 20, 50, and 100 mV s^{-1}; ii) calculated areal capacitance as a function of the scan rate. C.i) Galvanostatic charge/discharge curves at current densities of 5, 10, 15, 20, and 25 mA cm^{-2}; ii) calculated areal capacitance as a function of the current density.

higher electrolyte and charge transfer resistance of the PPy/rGO coating compared with the deposited MnO_2. Indeed, the Nyquist plot recorded for the PPy/rGO-coated electrode (Figure S9, Supporting Information) features a 45° slope in the low-frequency region, indicating diffusion-limited behavior which might account for the lesser performance of the PPy/rGO/Ni electrode in higher current densities.[48] Cycle stability of the PPy/rGO-coated electrode yielded 53% capacitance retention after 4000 cycles (Figure S10, Supporting Information), similar to previously reported electrodeposited PPy electrodes.[49]

2.3. Electrical and Mechanical Performance of an AMSC Comprising Hollow Ni Microfiber Electrodes

Figures 5 and **6** present the electrochemical and mechanical properties of an AMSC comprising a MnO_2/Ni cathode and PPy/rGO/Ni anode. Figure 5A shows the AMSC design. The electrolyte employed in the device was Na_2SO_4 interspersed within carboxymethyl cellulose gel.[50] A filter paper soaked with the gel electrolyte was used as a spacer and the device was encapsulated between two scotch tapes. Importantly, the entire AMSC device was compact and extremely thin (≈330 μm; Figure S11, Supporting Information).

Galvanostatic charge/discharge curves recorded in a voltage window of 1.5 V (Figure 5B) yield capacitance of 370 mF cm^{-2} at a current density of 1.5 mA cm^{-2}, which is high compared with recently published thin flexible MSCs.[19,33,41–43] When the current density was elevated to 25 mA cm^{-2}, a capacitance of 42 mF cm^{-2} was retained. This capacitance is more pronounced than previously reported MSCs, for example, devices based upon carbon nanotubes (4 mF cm^{-2} at current density of 0.125 mA cm^{-2}),[33] and PPy MSCs (10 mF cm^{-2} at a current density of 3.3 mA cm^{-2}).[43] The energy densities calculated

© 2018 WILEY-VCH Verlag GmbH & Co. KGaA, Weinheim

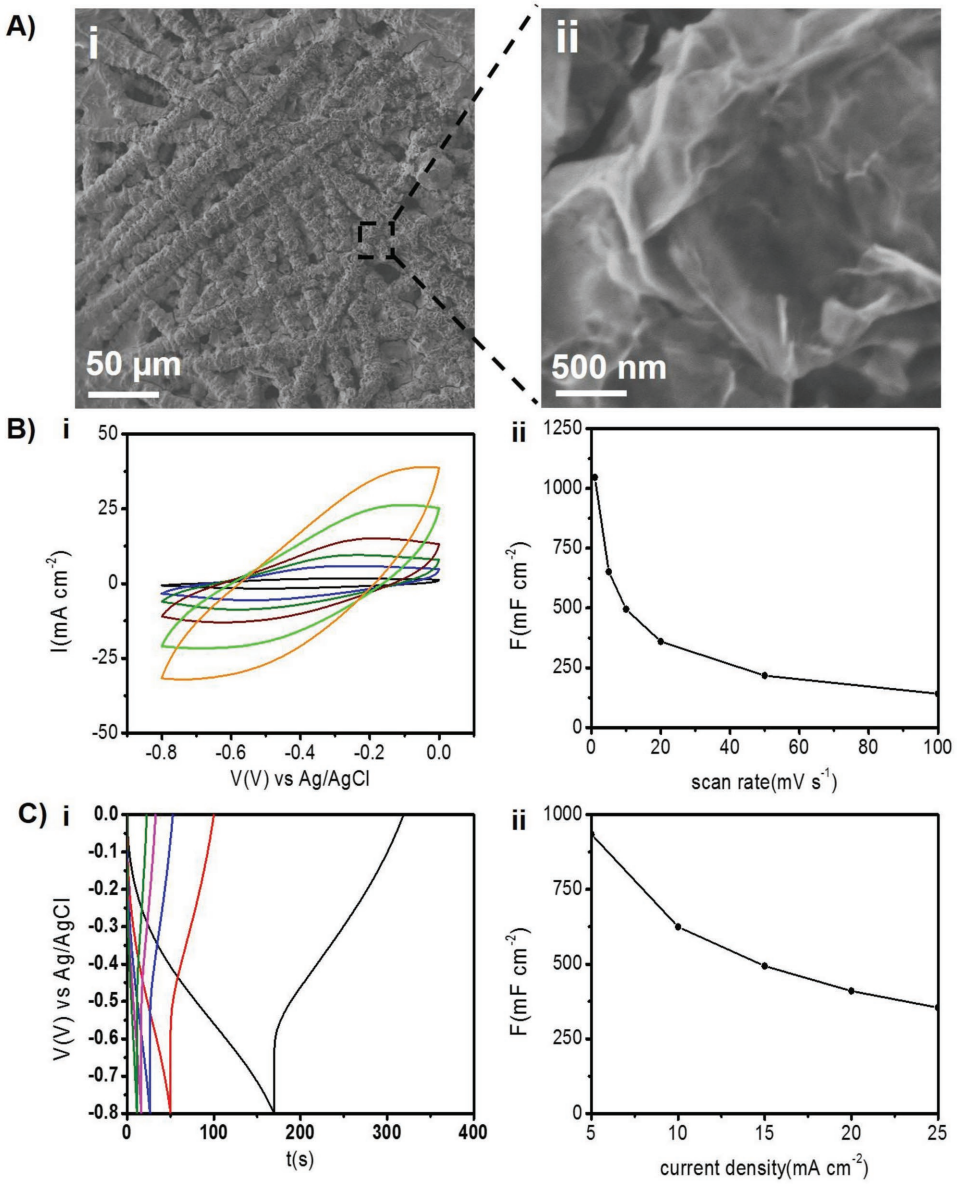

Figure 4. Characterization of the polypyrrole (PPy)/reduced graphene oxide (rGO)-coated Ni electrode. A) SEM images of the PPy/rGO-coated Ni electrode. B.i) Cyclic voltammetry of the PPy/rGO-coated Ni electrode using 1 M Na_2SO_4 as the electrolyte at scan rates of 1, 5, 10, 20, 50, and 100 mV s^{-1}; ii) calculated areal capacitance as a function of the scan rate. C.i) Galvanostatic charge/discharge curves at current densities of 5, 10, 15, 20, and 25 mA cm^{-2}; ii) calculated areal capacitance as a function of the current density.

are significantly high—0.112 and 0.013 mWh cm^{-2} for power densities of 2.25 and 37.5 mW cm^{-2}, respectively. Notably, these values attest to the potential of the Ni-microfiber AMSC to provide high-energy bursts.

It should be noted that the performance and operation parameters of the new nickel microtube AMSC device are on par or better than many previously reported flexible devices (Table S1, Supporting Information). In particular, inspection of Table S1 (Supporting Information) reveals that the freestanding nature of the Ni electrode enables assembly of a thin device exhibit comparable electrochemical performance to electrodes containing much higher loading of active materials, sometimes approaching thicknesses of thousands micrometer (an order of magnitude thicker).[27] The data presented in Table S1 (Supporting Information) underscore the high-capacitance values achieved by the AMSCs we developed, which are in the range of hundreds mF cm^{-2} while the corresponding capacitance values reported for numerous thin MSCs are, in fact, in the tens of mF cm^{-2} for the same charging rates.[19,33,41,42,51,52] Similarly, the Ragone plot in Figure 5C attests to the excellent areal energy of the Ni microtube AMSC, calculated as a function of the power densities, and shows the higher power densities that can be used by the AMSCs in comparison to previously reported MSCs.[19,33,41–43]

Considering the dimensions of the device, a volumetric capacitance of 1.3 F cm^{-3} at a current density of 750 mA cm^{-3}

© 2018 WILEY-VCH Verlag GmbH & Co. KGaA, Weinheim

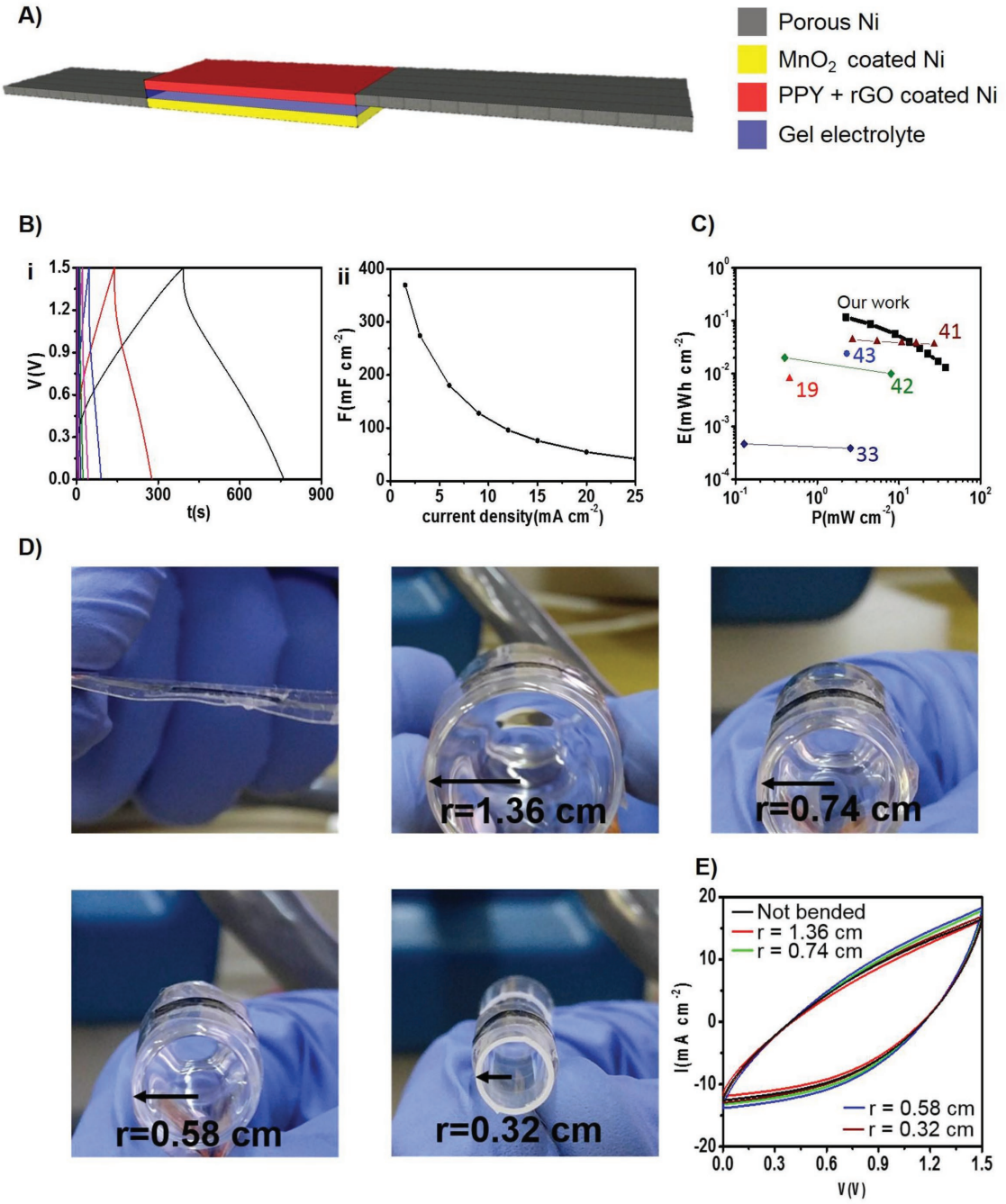

Figure 5. Electrochemical and mechanical performance of the asymmetric microsupercapacitor (AMSC). A) AMSC design. B.i) Galvanostatic charge/discharge curves at current densities of 1.5, 3, 6, 9, 12, 15, 20, and 25 mA cm^{-2}; ii) areal capacitance as a function of the current density. C) A Ragone plot depicting the areal energy density as a function of areal power density; datapoints obtained in this work are highlighted in bold. D) Digital photographs of the AMSC bended in different radii. E) Cyclic voltammetry (CV) curves, recorded at a scan rate of 50 mV s^{-1}, of the unbent AMSC, and bent in the different diameters shown in (D). The overlap between the CV curves indicates minimal change in electrochemical performance.

was calculated; this is an especially high value accounting for the fact that the final AMSC device is thin as the nickel electrode constitutes both the support substrate and current collector. The Nyquist plot, recorded at a frequency range of 100 kHz to 10 mHz, yields electrolyte resistance and charge transfer resistance of ≈10 and ≈20 Ω cm^2, respectively (Figure S12, Supporting Information), pointing to the potential of the device to work in high power densities. Notably, these resistance values are higher than the bare electrodes, due to the use of gel electrolyte compared with an aqueous electrolyte (in case of the bare electrodes). Cycle stability analysis, conducted at a current density of 12 mA cm^{-2}, produced excellent capacitance retention of 103% after 5000 cycles (Figure S13, Supporting Information).

© 2018 WILEY-VCH Verlag GmbH & Co. KGaA, Weinheim

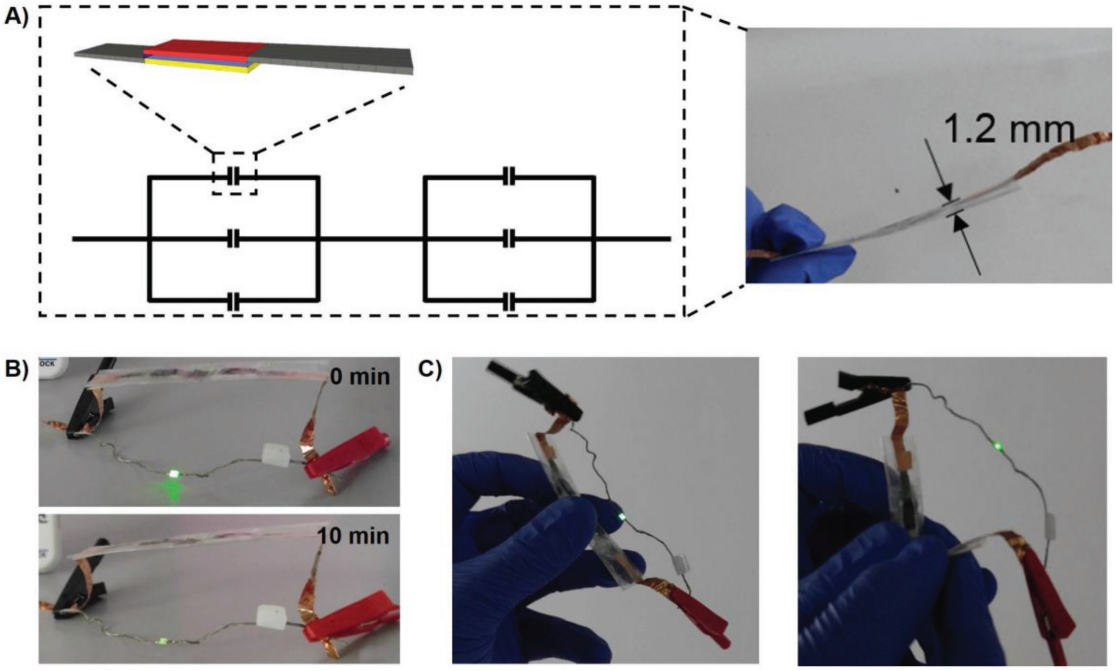

Figure 6. Linked AMSCs as an energy storage device. A) Diagram of the device, comprising three parallel-connected AMSCs, further linked in series with another three parallel-connected AMSCs. B) Using the device as an energy source to turn on a light-emitting diode (LED). High intensity observed immediately after connection (0 min); light is still generated even 10 min after operation of the device. C) Bending of the device did not affect the power generated and light intensity.

The experiments summarized in Figure 5D,E highlight the remarkable mechanical flexibility and resilience of the Ni microfiber–based AMSC. The photographs in Figure 5D show the AMSC bent upon solid tubes exhibiting different diameters (effectively yielding distinct device curvatures). Importantly, the CV curves recorded for the AMSCs having different curvatures show negligible changes in capacitance compared with the unbent device (Figure 5E), indicating that the extent of bending hardly affected the electrochemical performance of the AMSC. Overall, the electrical and mechanical features summarized in Figure 5 underlie the potential of the Ni microfiber-based AMSC to function as a useful energy source in flexible microelectronics.

To demonstrate usage of the hollow Ni microfiber-based AMSC as an energy source, a device composed of several AMSCs connected in parallel and series was assembled (Figure 6). Linking the AMSCs in parallel resulted in higher capacitance, whereas the series connection increased the voltage window of the device, overall yielding higher capacitance and operation voltage. Figure 6A illustrates the electric circuit diagram of the assembled device, where three AMSCs connected in parallel were linked in series to another three AMSCs connected in parallel. Importantly, the freestanding MnO_2/Ni and PPy/rGO/Ni electrodes can be stacked (in the parallel-connected AMSCs) on top of each other, still producing an overall extremely thin device (inset in Figure 6A); such stacking also provides a short diffusion path for electrolyte ions, resulting in higher overall capacitance.[53]

The galvanostatic charge/discharge curve of the assembled MSC at a current density of 3 mA cm^{-2} in Figure S14 (Supporting Information) confirms an excellent capacitance of around 370 mF cm^{-2}, corresponding to high energy of 0.463 mWh at a power of 9 mW. To demonstrate practical applicability of the device, we utilized the AMSC to turn on a green light-emitting diode (LED; Figure 6B). The photographs in Figure 6B demonstrate high initial light intensity, retained even after 10 min of continuous operation, reflecting the high energy density of the Ni microfiber–based device. Confirming the mechanical stability of the AMSC, the photographs in Figure 6C further demonstrate that significant bending did not adversely affect the light intensity of the LED.

3. Conclusions

We synthesized new freestanding high surface area electrodes comprising hollow nickel microfibers. The Ni microfiber electrodes constituted substrates for fabrication of MnO_2-coated cathode and PPy/rGO anode in a flexible asymmetric microsupercapacitor. Both the electrodes and the complete AMSC exhibited excellent electrochemical properties, including high areal capacitance at high current densities, cycle stability, and substantial areal energy and power densities. Thin AMSCs, prepared from the two electrodes and a gel electrolyte, could be integrated in a complex electrical circuit, generating high voltage and displaying remarkable flexibility and mechanical resilience. The hollow Ni microfiber electrodes may constitute a useful platform for diverse flexible devices in varied microelectronic applications.

© 2018 WILEY-VCH Verlag GmbH & Co. KGaA, Weinheim

4. Experimental Section

Materials: $Mn(Ac)_2{\cdot}4H_2O$, $NaH_2PO_4{\cdot}H_2O$, $SnCl_2$, $PdCl_2$, PS, $NaNO_3$, $KMnO_4$, pyrrole, and citric acid were purchased from Sigma Aldrich. H_2O_2 and graphite flakes were purchase from Alfa. $NiSO_4{\cdot}6H_2O$ was purchased from LOBA Chemie. DMF, HCl 32 wt%, and H_2SO_4 96 wt% were purchased from BioLab LTD. All chemicals were used as received. The water used in the experiments were doubly purified by a Barnstead D7382 water purification system (Barnstead Thermolyne, Dubuque, IA), at 18.3 MΩ resistivity.

Synthesis of Nickel Electrode: PS fibers were electrospun from a PS solution in DMF (30% w/v), on a glass for 40 min (under a 20 kV voltage and 22 cm between needle and collector) and were annealed at 100 °C for 15 min. Following electrospinning, carboxylation of the PS microfibers was carried out[35] by placing the PS fibers at 70 °C in a 0.6 M H_2SO_4 solution containing $KMnO_4$ (50 g L^{-1}) for 10 min. MnO_2 precipitate was removed by immersing the PS fibers in a 6 M HCl for 30 min. The PS fibers were then placed in a 0.12 M HCl solution containing $SnCl_2$ (4 g L^{-1}) for 20 min and for another 20 min in 0.06 M HCl solution containing $PdCl_2$ (40 mg L^{-1}). Between each step, the fibers were rinsed with water three times.

For the electroless deposition of Ni, the fibers were immersed in a 200 mL solution containing $NiSO_4{\cdot}6H_2O$ (20 g L^{-1}) and citric acid (10 g L^{-1}). The solution was heated to 70 °C and the pH was adjusted to 10.0 using ammonia. A 40 mL solution containing $NaH_2PO_4{\cdot}H_2O$ (38 g L^{-1}) was added slowly and the solution was left at 70 °C for 30 min. The nickel-coated PS fibers were then rinsed with distilled water three times. Subsequent electrodeposition of Ni was conducted for 15 min at 7 V in a two-electrode setup with Pt as the counter electrode in a solution containing $NiSO_4{\cdot}6H_2O$ (20 g L^{-1}) and NH_4Cl (6 g L^{-1}). Finally, the PS cores of the Ni microfibers were removed by immersing the sample in toluene.

Synthesis of Graphene Oxide: Graphene oxide was synthesized through a modified Hummers method.[54] One gram of graphite flakes were added to a beaker containing 46 mL of H_2SO_4 cooled in an ice bath. The mixture was then stirred for 1 h to disperse the graphite. After shifting the flask to a water bath, 1 g of $NaNO_3$ and 6 g of $KMnO_4$ were added slowly (within 15 min). The temperature of the water bath was increased to 40 °C and stirred for another 3 h. 50 mL of deionized water was slowly added to the reaction mixture, followed by 5 mL H_2O_2. Stirring was continued for further 10 min. The reaction mixture was then centrifuged (5000 rpm, 20 min) to separate the precipitate. Centrifugation was repeated until the supernatant showed a neutral pH. Resulting brown-colored residue of graphene oxide was immersed in liquid nitrogen and freeze-dried using lyophilizer. The GO was stored at 4 °C.

Synthesis of Nickel Electrodes Coated with MnO_2 or PPy/rGO: Both depositions were carried out in a three-electrode system with Ni electrode as the working electrode, Pt wire as counter electrode, and Ag/AgCl as reference electrode at 1.5 V for 12 min. The MnO_2 precursor solution contained 0.5 M $Mn(CH_3COO)_2$ and 0.5 M Na_2SO_4. The PPy/rGO precursor solution contained 0.4 M pyrrole and GO (8 mg mL^{-1}).

Preparation of Asymmetric Microsupercapacitor With Gel Electrolyte: First, a gel electrolyte was prepared by dissolving carboxymethyl cellulose (1.5 g) and Na_2SO_4 (2 g) in 30 mL of water at 85 °C overnight.[50] The device was assembled by attaching one electrode to a scotch tape. A filter paper soaked in the gel electrolyte was placed upon the electrode and then another electrode on top of the filter paper. Sealing of the device was done with another scotch tape. All electric contacts were covered with epoxy to prevent contact with the electrolyte.

Electrochemical Characterization: For CV measurements, a three-electrode configuration was used. Nickel electrodes coated with either MnO_2 or PPY/rGO were used as working electrodes, platinum wire as counter electrode, and Ag/AgCl (in 3 M KCl) as reference. The measurements were conducted in a 1 M Na_2SO_4 solution at different scan rates or current densities for galvanostatic charge/discharge. Asymmetric devices measurements were characterized in a two-electrode configuration. All electrochemical experiments were conducted on a BioLogic SP-150 instrument (Seyssinet-Pariset, France).

The capacitance from the CV experiments was calculated using the following equation:

$$C = \frac{\int I(V)dV}{2 \cdot A \cdot \Delta V \cdot \upsilon} \quad (1)$$

where the integral of I over V is the area of the CV curve, A is the area of the electrode, ΔV is the operating potential window, and υ is the scan rate.

For galvanostatic discharge curves, the capacitance was calculated according to the following equation:

$$C = \frac{I \cdot \Delta t}{A \cdot \Delta V} \quad (2)$$

where I is the discharge current, Δt is the discharge time, A is the area of the electrode, and ΔV is the operating potential window.

The energy density was calculated according to the following equation:

$$E = \frac{1}{2} C \cdot \Delta V^2 \quad (3)$$

where C is the areal capacitance and ΔV is the operating potential window.

Power density was calculated through the following equation:

$$P = \frac{E}{\Delta t} \quad (4)$$

where E is the energy density and Δt is the discharge time.

Supporting Information

Supporting Information is available from the Wiley Online Library or from the author.

Acknowledgements

The authors are grateful to the Ministry of Science and Technology (Kamin Program) and to the Israel Science Foundation (Grant 2014-14) for generous financial support. Also they thank Dr. Natalya Froumin for assistance with the XPS measurements.

Conflict of Interest

The authors declare no conflict of interest.

Keywords

areal capacitance, asymmetric supercapacitors, electroless deposition, flexible microsupercapacitors, nickel electrodes

Received: August 30, 2018
Revised: October 16, 2018
Published online: November 19, 2018

[1] S. Li, Q. Zhong, J. Zhong, X. Cheng, B. Wang, B. Hu, J. Zhou, *ACS Appl. Mater. Interfaces* **2015**, *7*, 14912.
[2] C. S. Boland, U. Khan, C. Backes, A. O'Neill, J. McCauley, S. Duane, R. Shanker, Y. Liu, I. Jurewicz, A. B. Dalton, J. N. Coleman, *ACS Nano* **2014**, *8*, 8819.
[3] W. Wu, S. Bai, M. Yuan, Y. Qin, Z. L. Wang, T. Jing, *ACS Nano* **2012**, *6*, 6231.

 © 2018 WILEY-VCH Verlag GmbH & Co. KGaA, Weinheim

[4] Y. S. Rim, S. H. Bae, H. Chen, N. De Marco, Y. Yang, *Adv. Mater.* **2016**, *28*, 4415.
[5] S. Y. Kim, S. Park, H. W. Park, D. H. Park, Y. Jeong, D. H. Kim, *Adv. Mater.* **2015**, *27*, 4178.
[6] G. Zhou, F. Li, H.-M. Cheng, *Energy Environ. Sci.* **2014**, *7*, 1307.
[7] L. Liu, Q. Weng, X. Lu, X. Sun, L. Zhang, O. G. Schmidt, *Small* **2017**, *13*, 1701847.
[8] H. Xia, Q. Xia, B. Lin, J. Zhu, J. K. Seo, Y. S. Meng, *Nano Energy* **2016**, *22*, 475.
[9] B. Liu, J. Zhang, X. Wang, G. Chen, D. Chen, C. Zhou, G. Shen, *Nano Lett.* **2012**, *12*, 3005.
[10] P. Yang, W. Mai, *Nano Energy* **2014**, *8*, 274.
[11] M. S. Kim, B. Hsia, C. Carraro, R. Maboudian, *Carbon* **2014**, *74*, 163.
[12] P. Simon, Y. Gogotsi, *Nat. Mater.* **2008**, *7*, 845.
[13] M. Inagaki, H. Konno, O. Tanaike, *J. Power Sources* **2010**, *195*, 7880.
[14] V. Augustyn, P. Simon, B. Dunn, *Energy Environ. Sci.* **2014**, *7*, 1597.
[15] Z. Lin, E. Goikolea, A. Balducci, K. Naoi, P. L. Taberna, M. Salanne, G. Yushin, P. Simon, *Mater. Today* **2018**, *21*, 419.
[16] C. Shen, C.-P. Wang, M. Sanghadasa, L. Lin, *RSC Adv.* **2017**, *7*, 11724.
[17] H. Xiao, Z.-S. Wu, L. Chen, F. Zhou, S. Zheng, W. Ren, H.-M. Cheng, X. Bao, *ACS Nano* **2017**, *11*, 7284.
[18] C. Zhang, J. Xiao, L. Qian, S. Yuan, S. Wang, P. Lei, *J. Mater. Chem. A* **2016**, *4*, 9502.
[19] R. Guo, J. Chen, B. Yang, L. Liu, L. Su, B. Shen, X. Yan, *Adv. Funct. Mater.* **2017**, *27*, 1702394.
[20] M. Beidaghi, C. Wang, *Adv. Funct. Mater.* **2012**, *22*, 4501.
[21] M. Wang, X. Yu, Z. Wang, X. Gong, Z. Guo, L. Dai, *J. Mater. Chem. A* **2017**, *5*, 9488.
[22] K. Wang, H. Wu, Y. Meng, Z. Wei, *Small* **2014**, *10*, 14.
[23] A. Ferris, S. Garbarino, D. Guay, D. Pech, *Adv. Mater.* **2015**, *27*, 6625.
[24] L. Wang, H. Yang, X. Liu, R. Zeng, M. Li, Y. Huang, X. Hu, *Angew. Chem., Int. Ed.* **2017**, *56*, 1105.
[25] P. Lv, Y. Y. Feng, Y. Li, W. Feng, *J. Power Sources* **2012**, *220*, 160.
[26] D. Ghosh, C. K. Das, *ACS Appl. Mater. Interfaces* **2015**, *7*, 1122.
[27] L. Zhang, P. Zhu, F. Zhou, W. Zeng, H. Su, G. Li, J. Gao, R. Sun, C. P. Wong, *ACS Nano* **2016**, *10*, 1273.
[28] W. Yu, B. Q. Li, S. J. Ding, *Nanotechnology* **2016**, *27*, 075605.
[29] D. Wu, S. Xu, C. Zhang, Y. Zhu, D. Xiong, R. Huang, R. Qi, L. Wang, P. K. Chu, *J. Mater. Chem. A* **2016**, *4*, 11317.
[30] X. Peng, L. Peng, C. Wu, Y. Xie, *Chem. Soc. Rev.* **2014**, *43*, 3303.
[31] D. P. Dubal, N. R. Chodankar, D. H. Kim, P. Gomez-Romero, *Chem. Soc. Rev.* **2018**, *47*, 2065.
[32] K. Wang, X. Zhang, C. Li, X. Sun, Q. Meng, Y. Ma, Z. Wei, *Adv. Mater.* **2015**, *27*, 7451.
[33] L. Song, X. Cao, L. Li, Q. Wang, H. Ye, L. Gu, C. Mao, J. Song, S. Zhang, H. Niu, *Adv. Funct. Mater.* **2017**, *27*, 1700474.
[34] T. Uyar, F. Besenbacher, *Polymer* **2008**, *49*, 5336.
[35] N. Zammatteo, C. Girardeaux, D. Delforge, J. J. Pireaux, J. Remacle, *Anal. Biochem.* **1996**, *236*, 85.
[36] S. M. Popescu, A. J. Barlow, S. Ramadan, S. Ganti, B. Ghosh, J. Hedley, *ACS Appl. Mater. Interfaces* **2016**, *8*, 31359.
[37] A. Morag, J. Y. Becker, R. Jelinek, *ChemSusChem* **2017**, *10*, 2736.
[38] N. P. Sari, D. Dutta, A. Jamaluddin, J.-K. Chang, C.-Y. Su, *Phys. Chem. Chem. Phys.* **2017**, *19*, 30381.
[39] M. Toupin, T. Brousse, D. Bélanger, *Chem. Mater.* **2004**, *16*, 3184.
[40] T. M. Dinh, A. Achour, S. Vizireanu, G. Dinescu, L. Nistor, K. Armstrong, D. Guay, D. Pech, *Nano Energy* **2014**, *10*, 288.
[41] H. Xu, X. Hu, H. Yang, Y. Sun, C. Hu, Y. Huang, *Adv. Energy Mater.* **2015**, *5*, 1401882.
[42] Z. Zhang, F. Xiao, J. Xiao, S. Wang, *J. Mater. Chem. A* **2015**, *3*, 11817.
[43] H. Park, J. W. Kim, S. Y. Hong, G. Lee, D. S. Kim, J. Oh, S. W. Jin, Y. R. Jeong, S. Y. Oh, J. Y. Yun, J. S. Ha, *Adv. Funct. Mater.* **2018**, *28*, 1707013.
[44] Y. Yang, Q. Huang, L. Niu, D. Wang, C. Yan, Y. She, Z. Zheng, *Adv. Mater.* **2017**, *29*, 1606679.
[45] Y. Chen, B. Xu, J. Wen, J. Gong, T. Hua, C.-W. Kan, J. Deng, *Small* **2018**, *14*, 1704373.
[46] H.-H. Chang, C.-K. Chang, Y.-C. Tsai, C.-S. Liao, *Carbon* **2012**, *50*, 2331.
[47] A. Morozan, P. Jégou, S. Campidelli, S. Palacin, B. Jousselme, *Chem. Commun.* **2012**, *48*, 4627.
[48] S. G. Mohamed, T.-F. Hung, C.-J. Chen, C. K. Chen, S.-F. Hu, R.-S. Liu, *RSC Adv.* **2014**, *4*, 17230.
[49] R. K. Sharma, A. C. Rastogi, S. B. Desu, *Electrochim. Acta* **2008**, *53*, 7690.
[50] N. R. Chodankar, D. P. Dubal, G. S. Gund, C. D. Lokhande, *Electrochim. Acta* **2015**, *165*, 338.
[51] L. Li, J. Zhang, Z. Peng, Y. Li, C. Gao, Y. Ji, R. Ye, N. D. Kim, Q. Zhong, Y. Yang, H. Fei, G. Ruan, J. M. Tour, *Adv. Mater.* **2016**, *28*, 838.
[52] S. Xu, Y. Dall'Agnese, G. Wei, C. Zhang, Y. Gogotsi, W. Han, *Nano Energy* **2018**, *50*, 479.
[53] D. Pech, M. Brunet, H. Durou, P. Huang, V. Mochalin, Y. Gogotsi, P.-L. L. Taberna, P. Simon, *Nat. Nanotechnol.* **2010**, *5*, 651.
[54] W. S. Hummers, R. E. Offeman, *J. Am. Chem. Soc.* **1958**, *80*, 1339.

 © 2018 WILEY-VCH Verlag GmbH & Co. KGaA, Weinheim